Food Chemistry 403 (2023) 134390

Contents lists available at ScienceDirect

Food Chemistry

journal homepage: www.elsevier.com/locate/foodchem

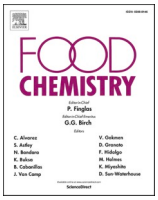

Effect of starch addition on the physicochemical properties, molecular interactions, structures, and *in vitro* digestibility of the plant-based egg analogues

Zhou Lu [a], Yi Liu [a,b], Yi En Jayne Lee [a], Andrew Chan [c], Pin-Rou Lee [d], Hongshun Yang [a,b,*]

[a] Department of Food Science & Technology, National University of Singapore, Singapore 117542, Singapore
[b] National University of Singapore (Suzhou) Research Institute, 377 Lin Quan Street, Suzhou Industrial Park, Suzhou, Jiangsu 215123, PR China
[c] Plant and Food Research, 120 Mt Albert Road, Sandringham, Auckland 1025, New Zealand
[d] Aztech Technologies Pte Ltd., 31 Ubi Road 1, #01-05, Singapore 408694, Singapore

ARTICLE INFO

Keywords:
Egg analog
Alternative protein
Starch
Gelation
Molecular interaction
Molecular structure

ABSTRACT

This study investigated the gelling mechanisms of plant-based eggs modified with corn starch (CS), glutinous rice starch (GS), or potato starch (PS) at soy protein isolate (SPI)/starch ratios of 10:4, 8:6, and 6:8 (w/w). A plant-based omelet with SPI/PS 8:6 matched the texture (especially cohesiveness (0.75 vs 0.79)) and specific volume (1.28 vs 1.32 cm^3/g) of an egg omelet best. This was attributed to greater protein-starch interactions (H-bonding, ionic bonding) that supported its strong structure. SPI/CS 8:6, SPI/GS 8:6, SPI/PS 10:4, and SPI/PS 6:8 demonstrated more ruptured granules and formed weaker gels. These proposed models were verified by nuclear magnetic resonance (NMR)-based metabolomics, where the stronger SPI/PS 8:6 gel released less metabolites after *in vitro* digestion. Through understanding different roles of starch in plant-based egg systems, this study suggests more potential applications of starch in modifying food properties.

1. Introduction

Texture is a key physicochemical property for determining a food's quality during consumption. For example, the characteristic texture of a native egg omelet is light, spongy, and springy. This can be ascribed to its cooking process, during which the moisture in the egg is converted into steam, the incorporated air bubbles expand, and the egg proteins coagulate. The steam is then trapped in the coagulated protein matrix that imparts a fluffy texture to omelet products (McGee, 2007).

Apart from the cooking condition, texture is closely related to food composition. Plant proteins are the main components of plant-based eggs. However, since plant proteins have less likely to form protein networks than animal proteins (Kamani, Meera, Bhaskar, & Modi, 2019), their presence might reduce the strength and elasticity of resulting plant-based egg products. Such inadequacy was also observed for the plant-based meat products, where the weaker structural networks formed by plant proteins diminished their resistance to compression (Kamani et al., 2019; Youssef & Barbut, 2011). In the egg category, Zhang et al. (2019) pointed out that the incorporation of soy proteins into egg proteins led to less stable conformations as compared to only egg proteins. Similarly, Su et al. (2015) reported that soy proteins could interfere with the network formation in the egg white emulsion, resulting in softer and less springy texture of egg-based gels.

Molecular interactions and the resulting structures also play a part in texture formations. The Cauchy-Born theory has related gel rigidness and elasticity with molecular interactions: $G' = 4n_e\kappa\langle r^2\rangle$, where n_e is the number density of the elastically-active bonding, κ is the bonding stiffness, and $\langle r^2\rangle = \frac{1}{3}\int(r_x r_y + r_y r_z + r_x r_z)P(r)dr$ is the length scale related to the elastically-connected regions (Alexander, 1998). Subsequently, Whitaker et al. (2019) and Wang, Chen, Yang, and Cui (2017) have

Abbreviations: PS, potato starch; CS, corn starch; GS, glutinous rice starch; SPI, soy protein isolate; NE, native egg; SV, specific volume; LVR, linear viscoelastic region; DI, deionized; FTIR, Fourier transform infrared; DP, degree of polymerization; XRD, X-ray diffraction; RC, relative crystallinity; SEM, scanning electron microscope; NMR, nuclear magnetic resonance; TSP, sodium 3-trimethylsilyl [2,2,3,3-d4] propionate; FC, fold change; LA, linoleic acid; OA, oleic acid; PA, palmitic acid; α-D-glc, α-D-glucose; β-D-glc, β-D-glucose; PCA, principal component analysis; OPLS-DA, orthogonal projection to latent structure-discriminant analysis; VIP, variable importance in projection.

* Corresponding author at: Department of Food Science & Technology, National University of Singapore, Science Drive 2, Singapore 117542, Singapore.
E-mail address: fstynghs@nus.edu.sg (H. Yang).

https://doi.org/10.1016/j.foodchem.2022.134390
Received 24 June 2022; Received in revised form 17 September 2022; Accepted 20 September 2022
Available online 24 September 2022

correlated gel structures with textural attributes. Whitaker et al. (2019) noted that locally dense clusters of particles are conducive to the linear elasticity of gels, in which each cluster is a rigid and mechanical unit that can propagate elastic deformations. Wang et al. (2017) found that gels with higher springiness are broken into a few large fragments after the first compression in textural profile analysis (TPA), while those with lower springiness are broken into many small fragments.

Current eggless products are limited by some textural characteristics. For example, a decreased springiness was observed when plant proteins were used to substitute egg in cake formulations (Lin, Tay, Yang, Yang, & Li, 2017; Shao, Lin, & Chen, 2015). According to our previous work, eggless omelets prepared by chickpea flour and soy protein isolate were poor in springiness texture from TPA, along with a lack of elastic mouthfeel from the preliminary sensory evaluation (Lu, Lee, & Yang, 2022). One of the methods for improving the textural attributes is to add starch, which was successful in other plant-based food systems (e.g., corn, potato, tapioca, wheat, and waxy rice starch in meat replacers (Bühler, Schlangen, Möller, Bruins, & van der Goot, 2022), rice and tapioca starch in yogurts (Grasso, Alonso-Miravalles, & O'Mahony, 2020), corn and tapioca starch in cheese (Mattice & Marangoni, 2020), etc.). Such improvements are generally based on the interactions between proteins and starch, which include associative interactions, steric hindrances, competitive hydration, and phase behaviors. These interactions are dependent on both the type and concentration of the added starch. For instance, Jekle, Mühlberger, and Becker (2016) reported that gluten formed a network in gluten-starch blends and thereby hindered the starch gelatinization process. However, Li et al. (2014) concluded that no significant interaction occurred between soy protein isolate and corn starch as the samples with the starch concentration higher than 50 % (d.b.) favored a phase separated matrix. Different interaction profiles could further influence the macro- and microstructure of protein gels and its products, and thus influence the physicochemical properties of the starchy foods.

Starch has an excellent water-binding capacity, laying a basis for the thickening, binding, adding body, and improving mouthfeel functionalities. A wide range of starch is widely available today, including corn starch, wheat starch, tapioca starch, potato starch, and rice starch. Different types of starch can have different contributions to food texture. Native potato starch and corn starch contain 20–30 % amylose (Mishra & Rai, 2006), while glutinous rice starch contains 1.0–2.3 % amylose. Amylose is a linear fraction that orients in parallel and allows more hydroxyl groups along the chains to approach each other, therefore a higher amylose composition could facilitate the gelling process (Mishra & Rai, 2006) and enhance the texture of farinaceous foods significantly (Schirmer et al., 2013). On the other hand, potato starch has a higher concentration of phosphate than other starches (Mishra & Rai, 2006), as well as larger granule sizes and lower gelatinization temperature. In addition, the negatively charged phosphate monoester groups in potato starch could generate the ionic repulsion that weakens the hydroxyl associations along the chains, and thus contributes to its increased water-binding capacity and swelling power (Mishra & Rai, 2006).

This study aimed to evaluate the impact of potato starch (PS), corn starch (CS), and glutinous rice starch (GS) on the physicochemical properties of the plant-based eggs, and more importantly, to investigate the mechanisms that account for the different modification effects among different starch. For these purposes, TPA, specific gravity and specific volume measurements, and rheological tests were carried out to describe the physicochemical properties. Dissociation treatments and Fourier transform infrared (FTIR) spectroscopy were conducted to determine the molecular interactions. Wide-angle powder X-ray diffraction (XRD) and FTIR spectroscopy were performed to depict the structures of starch granules. Scanning electron microscopic (SEM) analysis was used to observe microstructures in the respective gels. Last, NMR-based metabolomics was performed to analyze metabolite releases from the plant-based egg gels during *in vitro* digestion, further verifying the schematic models proposed from the points of molecular interactions and structures.

2. Materials and methods

2.1. Materials

Soy protein isolate (Myprotein®), chickpea flour (Dr Gram®), sunflower oil (Naturel®), and baking powder (Redman®) were procured from the online shops (Lazada, Singapore). Potato starch (PS) (Windmill®), corn starch (CS) (Windmill®), and glutinous rice starch (GS) (Erawan®) were procured from the local supermarket (Sheng Siong, Singapore). Other ingredients included mono-, diglycerides (Emulpals 110®, Palsgaard Asia Pacific Pte ltd, Singapore), transglutaminase (Ajinomoto®, Amazon, Seattle, USA), KCl (Now foods®, iHerb, Singapore), and κ-carrageenan (Better 4U Holdings Pte ltd, Singapore). The benchmark was native liquid egg (N&N®, N&N Agriculture Pte ltd). All ingredients were of food grade.

In addition, NaCl, urea, GuHCl, KBr, $CaCl_2$, NaOH, KCl, KH_2OP_4, $NaHCO_3$, $MgCl_2(H_2O)_6$, $(NH_4)_2CO_3$, HCl, α-amylase (from porcine pancreas, 10 U/mg), pepsin (from porcine gastric mucosa, 4177 U/mg), pancreatin (from porcine pancreas, containing amylase, trypsin, lipase, ribonuclease, and protease; 96.7 U/mg based on trypsin activity), amyloglucosidase, and bile were purchased from Sigma-Aldrich (Singapore). All chemicals were analytical grade.

2.2. Sample preparation

The formulations of the plant-based eggs were modified from our earlier publication (Lu, Lee, & Yang, 2022) with the addition of corn starch (CS), glutinous rice starch (GS), or potato starch (PS) at various ratios. Specifically, 14 % of soy protein isolate/starch blended at different weight ratios (SPI/PS 8:6, SPI/CS 8:6, SPI/GS 8:6, SPI/PS 10:4, SPI/PS 6:8), 4.6 % of chickpea flour, 1 % of baking powder, 0.5 % of mono-, diglyceride, 0.3 % of κ-carrageenan, 0.1 % of KCl, 0.025 % of transglutaminase, 5.6 % of oil, and 73.875 % of water were blended at 20,000 rpm for 6 min with an electric blender (Mayer®, Singapore) to form the plant-based eggs.

The native and plant-based omelets were prepared American style as published previously (Lu, Lee, & Yang, 2022). Briefly, 100 g of the eggs were transferred onto a frypan (Lamart®, Singapore) containing 5 g of sunflower oil and pre-heated at 130 °C for 2.5 min. Then the egg sample was heated at 130 °C for 2.5 min, followed by being flipped over to heat for another 1 min. Afterwards, the omelets were cooled for 1 h at room temperature before further testing.

The native and plant-based egg gels were prepared by heating the eggs at 90 °C for 30 min, and then maturing the gels at 4 °C for 12 h before further testing (Lu, Lee, & Yang, 2022). Similarly, the native starch solutions (6 %) were heated at 90 °C for 30 min and matured at 4 °C for 12 h followed by freeze-drying for FTIR analyses.

2.3. Physicochemical properties of the plant-based eggs

2.3.1. Textural properties

The textural properties of the pie-shape omelet pieces (cut by a 20 mm diameter ring mold) were determined with a TA-XT2i texture analyzer (Stable Micro System ltd., Surrey, UK) fitted with a P/35 probe as described by Lu, Lee, and Yang (2022). The textural attributes were determined from force-time curves.

2.3.2. Air holding properties

The specific gravity of the eggs was measured as published earlier (Lin et al., 2017). The mass of the eggs filled in a cup with certain cubage was marked down with respect to the mass of DI water filled in the same cup, and the specific gravity was determined as:

$$\text{Specific gravity} = \frac{\text{Mass of the eggs at } 25^{\circ}\text{C}}{\text{Mass of DI water at } 25^{\circ}\text{C}} \quad (1)$$

The volume of the omelets was determined by scanning five stacking omelet pieces with a Stable Microsystem Volscan profiler 600 (Stable Micro Systems ltd., Surrey, UK). The specific volume was calculated as described by Lin et al., 2017:

$$\text{Specific volume} = \frac{Volume}{Mass} \quad (2)$$

2.3.3. Rheological properties of the plant-based eggs

The rheological properties were analyzed with a rotational stress-controlled rheometer (MCR 102, Anton Paar, Graz, Austria) equipped with a Peltier temperature controller, and fitted with a parallel plate (diameter = 25 mm, gap = 1.0 mm). Samples were equilibrated at 20 °C for 30 min before being transferred to the rheometer for the rheological testing:

(1) a temperature sweep conducted at the frequency of 1 Hz and the strain of 0.1 % (within LVR) as described by Sui et al. (2015). During the sweep, samples were firstly held at 50 °C for 60 s, heated from 50 °C to 95 °C at 0.22 °C/s, held at 95 °C for 150 s, then cooled to 50 °C at 0.22 °C/s and held for another 120 s;
(2) gel maturation at 20 °C for 30 min;
(3) a strain sweep from 0.01 to 100 % performed at the frequency of 1 Hz and at 20 °C.

2.4. Molecular interaction analysis

The molecular interactions involved in the plant-based omelets were determined according to Zhang et al. (2016) with modifications. Specifically, the omelet samples were treated with 1) 0.05 mol/L NaCl solution (solution A); 2) 0.6 mol/L NaCl solution (solution B); 3) 0.6 mol/L NaCl solution + 1.5 mol/L urea solution (solution C); and 4) 0.6 mol/L NaCl solution + 8.0 mol/L urea solution (solution D). The ionic bonding, hydrogen bonding, and hydrophobic interactions were inferred by the difference in solubilized protein content between solution B and A, solution C and B, and solution D and C, respectively. Plant-based omelet samples (2.00 g ± 0.02 g) were chopped and homogenized with each solution at 8,000 rpm for 1 min (D-130 model, Wiggens Co., ltd, Beijing, China). Then the treated samples were incubated at 4 °C for 60 min, and centrifuged at 5,000 *g* for 10 min. The solubilized concentrations were determined using the Bradford method.

2.5. FTIR spectroscopy analysis

The lyophilized native starch and plant-based egg gel powders were taken through FTIR analysis according to Lu, Lee, and Yang (2022). The pellets were prepared by mincing sample powders with KBr in a ratio of 3 mg: 97 mg, and the FTIR spectra were obtained from 4500 to 450 cm^{-1} with a Spectrum One FTIR spectrometer (PerkinElmer, Waltham, MA, USA). All spectra were normalized, and baseline corrected in the PerkinElmer Spectrum IR software (PerkinElmer, Waltham, MA, USA). Fourier self-deconvolution was applied over the 1100–950 cm^{-1} region with the Omnic software 8.2 (Thermo Fisher Scientific Inc. Waltham, MA, USA).

2.6. Wide angle powder X-ray diffraction (XRD) analysis

The lyophilized native starch and plant-based egg powders followed XRD analysis according to Lin et al. (2017). XRD patterns were collected over the 2θ range of 5-30°, step size of 0.01°, and the measuring time of 1 s per 2θ interval with a Siemens D5005 diffractometer (Bruker AXS, Karlsruhe, Germany) fitted with a copper anode tube operated at 40 kV and 40 mA. For data processing, baseline subtraction, $K\alpha_2$ peak stripping, and area integration were performed with the Jade 6.0 software (Materials Data JADE, Livermore, CA, USA). The relative crystallinity of the starchy samples was calculated as:

$$X_C = \frac{A_c}{A_c + A_a} \quad (3)$$

where, X_C is the relative crystallinity, A_c is the sum of the integrated area of the crystalline regions, and A_a is the integrated area of the amorphous region.

2.7. Scanning electron microscopy (SEM) analysis

The microstructures of the plant-based egg gels were visualized according to Huang et al. (2021) with modifications. The lyophilized plant-based egg gel powders were sprayed onto an aluminum plate attached with a double-sided carbon sticky tape. Samples were coated with a film gold to improve sample conductivity. Afterwards, the samples were observed using a Field Emission Scanning Electron Microscope (FESEM, JEOL JSM-6701F) operated at 15 kV accelerating voltage, and the images were captured at a magnification of 300×.

2.8. Metabolite release of the plant-based egg gels

2.8.1. In vitro digestion

The plant-based egg gels were digested through a simulated three-stage *in vitro* process based on a modified method (Huang et al., 2021). The simulated electrolyte fluids were prepared accordingly.

In the simulated oral phase, the mixed enzyme solution containing 4 mL of α-amylase solution (in simulated salivary fluid with enzyme activity of 75 U/mL), 975 μL of DI water, 25 μL of 0.3 mol/L $CaCl_2$, and 15 μL of 1 mol/L hydrochloric acid (for adjusting pH) was firstly pre-warmed to 37 °C. Then 2.5 g of the egg gels was incubated in the mixed enzyme solution at 37 °C for 2 min (with shaking at 200 rpm). In the simulated gastric phase, the mixed enzyme solution containing 8 mL of pepsin solution (in simulated gastric fluid with enzyme activity of 2000 U/mL), 1.345 mL of DI water, 650 μL of 1 mol/L hydrochloric acid (for adjusting pH to 3.0), and 5 μL of 0.3 mol/L $CaCl_2$ was pre-warmed to 37 °C. The mixed solution was then added into the digestive products, followed by incubation at 37 °C for 2 h (with shaking at 200 rpm). In the simulated intestinal phase, the mixed enzyme solution containing 16 mL of pancreatin solution (in simulated intestinal fluid with enzyme activity of 100 U/mL based on trypsin activity), 3.48 mL of DI water, 0.1768 g of bile, 400 μL of 1 mol/L NaOH (for adjusting pH to 7.0), 80 μL of amyloglucosidase solution, and 40 μL of 0.3 mol/L $CaCl_2$ was pre-warmed to 37 °C. The mixed solution was then added into the digestive products, followed by incubation at 37 °C for 2 h (with shaking at 200 rpm). The digestive products were subsequently transferred in the boiling water immediately for enzyme deactivation.

2.8.2. Nuclear magnetic resonance (NMR) spectroscopic analysis

The *in vitro* digested products were further treated and analyzed according to Huang et al. (2021). Firstly, the inactivated digestive products were centrifuged at 10,000 *g* for 5 min, and the collected supernatants were filtered with a 0.45 μm hydrophilic microporous membrane. Next, 1 mL of the purified supernatants were lyophilized for 5 days, and the lyophilized products were dissolved in 990 μL of deuterated water (D_2O, 99.9 %) and 10 μL of 2.0 % sodium 3-trimethylsilyl [2,2,3,3-d4] propionate (TSP), followed by centrifugation at 12,000 *g* for 10 min. Afterwards, 600 μL of the supernatants was pipetted into the NMR tubes (diameter = 5 mm) for further testing.

The metabolite release was analyzed with an NMR spectrometer (DRX-500, Bruker, Rheinstetten, Germany) at the frequency of 500.23 MHz. The 1D ^{1}H spectra were collected at the standard NOESY setting (noesypr1d), the scan number of 128, and the automatic pulse calculation (pulsecal) for 90° pulse length optimization. Furthermore, the 2D ^{1}H–^{13}C heteronuclear single quantum coherence spectroscopy was

performed with the Bruker hsqcedetgpsisp2.3 pulse sequence for detailed metabolic identifications. The 1D ^{1}H spectra (width = 10.0 ppm) were obtained from the F2 channel while the 2D ^{1}H–^{13}C spectra (width = 180.0 ppm) were from the F1 channel.

2.8.3. Spectra processing and analyses

The NMR spectra were processed and analyzed as published earlier (Huang et al., 2021). Firstly, the baseline corrections and phase distortions were performed on the 1D ^{1}H spectra with the Mnova software (Mestreab, Research SL, Santiago de Compostela, Spain). Metabolite identifications were conducted in cooperation of the 2D ^{1}H–^{13}C spectra, during which chemical shifts were checked in Biological Magnetic Resonance Data Bank (https://www.bmrb.wisc.edu/metabolomics), Madison Metabolomics Consortium Database (https://mmcd.nmrfam.wisc.edu), and Human Metabolome Database (https://www.hmdb.ca/), and relative references (Huang et al., 2021; Vidal et al., 2016). The identified peaks (0.0–10.0 ppm) within the 1D ^{1}H spectra were normalized relative to the TSP peak (0.0 ppm), with the residual water resonance region (4.76–5.00 ppm) being excluded from analysis. The region buckets (width = 0.01 ppm) were extracted, and the binned data were captured from the 1D ^{1}H spectra.

The binned data were subjected to the principal component analysis (PCA) and the orthogonal projection to latent structure-discriminant analysis (OPLS-DA) with the SIMCA software (version 13.0, Umetrics, Umeå, Sweden). Variable importance in projection (VIP) values, the fold changes (FCs) and the *P*-values of the metabolites were determined for the pairwise groups.

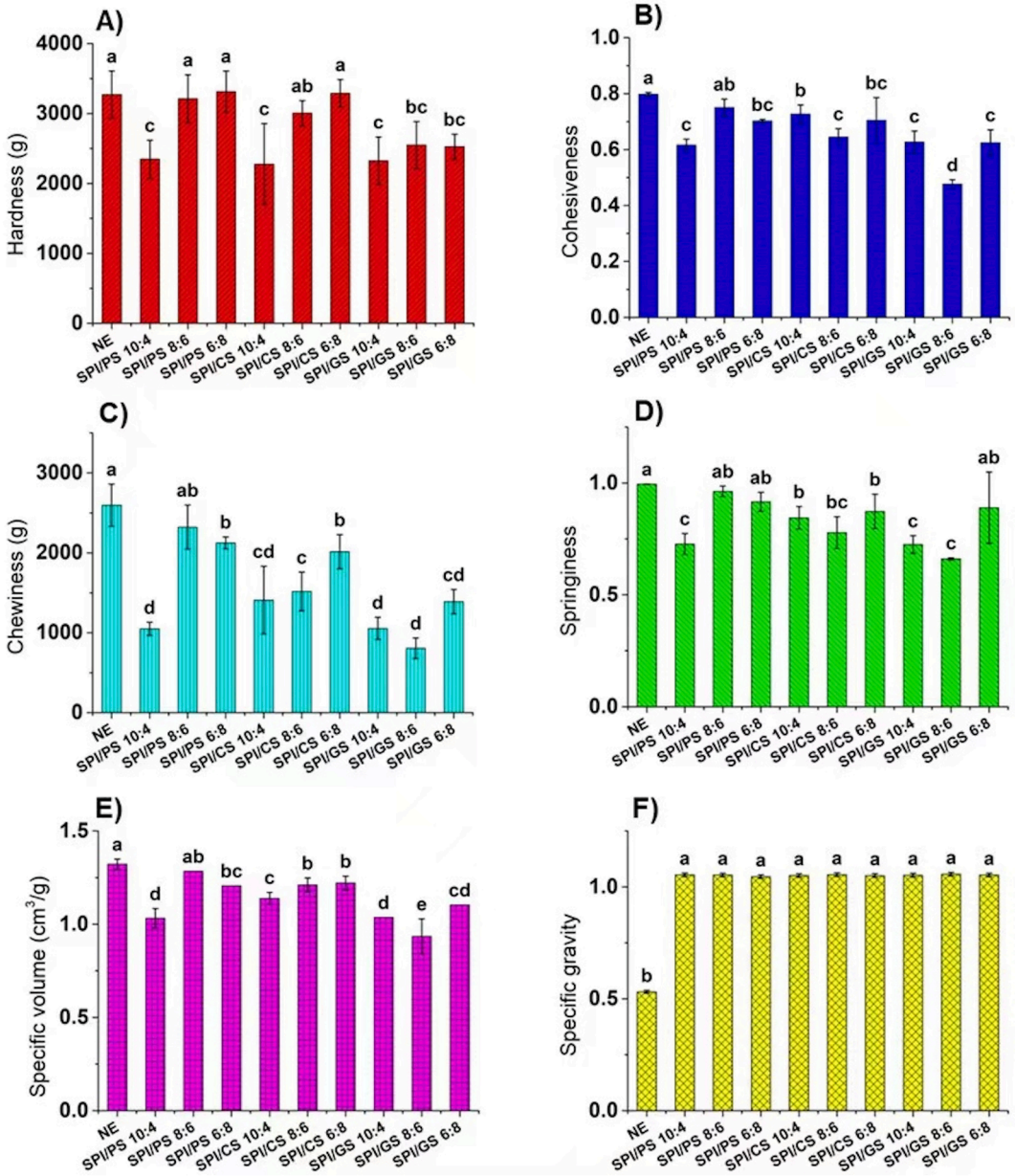

Fig. 1. Effect of the types of starch and soy protein isolate/starch ratios on the hardness (A), cohesiveness (B), chewiness (C), springiness (D), specific gravity (E), and specific volume (F) of the plant-based omelets in comparison of the native egg (NE) omelet. *Groups with different letters indicate significant difference ($P < 0.05$). *SPI/PS 10:4, SPI/PS 8:6, SPI/PS 6:8, SPI/CS 10:4, SPI/CS 8:6, SPI/CS 6:8, SPI/GS 10:4, SPI/GS 8:6, and SPI/GS 6:8 refer to the plant-based eggs with the addition of 10 % soy protein isolate and 4 % potato starch, 8 % soy protein isolate and 6 % potato starch, 6 % soy protein isolate and 8 % potato starch, 10 % soy protein isolate and 4 % corn starch, 8 % soy protein isolate and 6 % corn starch, 6 % soy protein isolate and 8 % corn starch, 10 % soy protein isolate and 4 % glutinous rice starch, 8 % soy protein isolate and 6 % glutinous rice starch, and 6 % soy protein isolate and 8 % glutinous rice starch (w/w), respectively.

2.9. Statistical analysis

All analyses were performed independently and at least in triplicate. Results were expressed as mean or mean ± standard deviations. Statistic significant differences were determined with one-way ANOVA with post-hoc Bonferroni test in the SPSS Statistics 20 software (IBM, Chicago, IL, USA), and $P < 0.05$ (two-tailed) was defined as statistically significant.

3. Results and discussion

3.1. Physicochemical properties of the plant-based eggs

3.1.1. Textural properties

The textural profile of the plant-based eggs modified by the various ratios of SPI/potato starch (PS), SPI/corn starch (CS), or SPI/glutinous rice starch (GS) are presented in Fig. 1A-D. Even though PS and CS at SPI/starch ratios of 8:6 and 6:8 can enhance the hardness of the plant-based eggs to a comparable level as the native egg (Fig. 1A), their effects on other attributes were different. PS-modification at SPI/PS 8:6 reached the springiness, cohesiveness, and chewiness of the native egg omelet, while CS- or GS-modifications at SPI/starch 8:6 were inferior in these attributes (Fig. 1B-D). This observation could be attributed to the different natures of the different types of starch, which led to different interactions and structures within the plant-based egg system. PS had the higher phosphorus content, which made it more capable of separating chains apart and allowing water access during gelatinization (Mishra & Rai, 2006).

In addition, the more hydroxyl groups engaged in hydrogen bonding formation between starch chains, and the more available water-binding sites of PS resulted in its higher water-binding capacity (10.44 g H_2O g^{-1}) than other starch (Mishra & Rai, 2006), thus contributing to the superiority in cohesiveness and springiness of the SPI/PS 8:6 system. Moreover, a study focusing on the functional properties of different starches also reported the higher cohesiveness and chewiness of the PS gel than those of the CS gel (Mishra & Rai, 2006); a phenomenon that was also observed in our TPA results. This could be ascribed to the higher polymerization degree of the amylose in PS (DP 6000; Mishra & Rai, 2006) that propelled it towards the gummy and cohesive texture.

As for the impacts of SPI/starch ratios on the texture profile of plant-based omelets, hardness, springiness, and chewiness generally increased with the increasing starch proportions. However, cohesiveness followed a different trend. PS-modified omelets attained the highest cohesiveness at the ratio of 8:6 where CS-modified and GS-modified omelets exhibited the lowest. This result indicated that at the critical SPI/starch ratio of 8:6, PS-modified omelet formed a relatively stable gel structure that could cohere the components better than other ratios. To further explore the mechanisms why PS-modified omelets showed the best textural profile at SPI/PS ratio of 8:6 and the difference among PS, CS, and GS at the SPI/starch ratio of 8:6, SPI/PS 10:4, SPI/PS 8:6, SPI/PS 6:8, SPI/CS 8:6, and SPI/GS 8:6 were subjected to the further technical analyses.

3.1.2. Specific gravity and specific volume

The specific gravity of the eggs and the specific volume of the omelets are presented in Fig. 1E and Fig. 1F, respectively. Substitution with the plant-based egg formulations augmented the specific gravity from 0.53 for the native egg to 1.06 (Fig. 1E), regardless of the type and the concentration of the added starch. This clearly indicated that the plant-based eggs were inferior in foaming compared to native eggs, which is important in providing the 'light' mouthfeel with the omelet products. Despite the inadequacy in its foaming abilities, the plant-based omelet with SPI/PS 8:6 held the commensurable specific volumes ($P > 0.05$) to the native egg omelet (Fig. 1F), mainly because the CO_2 released from the leavening agents could be trapped by its stronger plant-based egg gels formed during heating. In analogy to bakery products, the volumes of the omelet products were stabilized by the egg proteins that were able to form strong thermal gels to guarantee structures (McGee, 2007). Despite the limitations of soy proteins in foaming and gelling, modifications with PS at SPI/PS 8:6 improved the specific volume to an equivalent level as the native egg omelet (Fig. 1F), largely related to its preponderance in strengthening the gel network (higher G'_{LVR} in Fig. 2C). In contrast, the lower gel strength (Fig. 2C) owing to the small content of amylose in GS (1.4 %) and the other SPI/PS ratios could explain their smaller specific volumes.

3.1.3. Viscoelastic properties

The large deformation behaviors of the plant-based eggs were characterized by the strain sweep (Fig. 2A). It was shown that the storage modulus (G') was higher than the loss modulus (G") for all the plant-based egg samples within the linear viscoelastic region (LVR), corresponding to the predominant elastic behavior in the structure. As G' was related to the elastic deformation of the system, the gel strength can be indicated from the G' value within the LVR (G'_{LVR}) when G' > G" (Moreno et al., 2020). Our results revealed that the PS- and CS-modified samples had the significant greater gel strength than the GS-modified sample (G'_{LVR} in Fig. 2C), following a coincident trend in the cohesiveness result (Fig. 1B) as cohesiveness was dependent on the tensile and compression strength of foods. The factor contributing to this finding could be that PS (27 %) and CS (25 %) contained more amylose than GS (1.4 %), a linear fraction that oriented in parallel and allowed more hydroxyl groups along the chains to approach each other, thereby facilitating the gelling process (Mishra & Rai, 2006). Regarding the additive amount, SPI/PS 8:6 imparted the greatest effect on the gel strength (Fig. 2C). With the increased PS ratio (from SPI/PS 10:4 to SPI/PS 8:6), the starch granules acted as the filling reinforcement agents and the water absorbing agents that increased the density of the protein matrix; this resulted in the more rigid gel with increased G' (Mounsey & O'Riordan, 2008). However, with the further increase in PS ratio (from SPI/PS 8:6 to SPI/PS 6:8), the gel strength was weakened (Fig. 2C). The relatively lower protein content in the SPI/PS 6:8 system may be inadequate to wrap the superfluous starch granules, which could diminish the proteins' impacts on restricting starch rupture (Lu, Donner, Yada, & Liu, 2016). Although the residual granule fragments (mainly contained amylopectin) were still able to fill inside the protein networks, their contributions to the gel strength were not as good as those with the lower PS ratios.

Furthermore, the thermal behaviors of the plant-based eggs were described by the temperature sweep over a heating–cooling cycle (Fig. 2B). In the heating phase, G' increased gradually as temperature increased, then attained the peak values (G'_{peak}) at around 85 °C; the hydration and swelling of the starch granules might account for such increase (Yang, Zhong, Douglas Goff, & Li, 2019). Upon further heating to 95 °C, G' declined, owing primarily to the rupture of the starch granules in this phase (Sui et al., 2015). The lowest $G'_{breakdown}$ value in the SPI/PS 8:6 system (Fig. 2C) evidenced the presumption that at this critical ratio, PS granules were well-embedded in the protein networks to retard rupture. This observation was also related to the highest gel strength of the SPI/PS 8:6 sample (Fig. 2C). Afterwards, G' increased gradually under the continuous heating at 95 °C, followed by a sharp increase in the cooling phase (95–50 °C) (Fig. 2B). The associative protein-starch interactions involved could further strengthen the gels upon cooling, thereby leading to the increased G'. As for the types of starch, SPI/CS 8:6 and SPI/GS 8:6 presented the higher $G'_{breakdown}$ values in comparison of SPI/PS 8:6 (Fig. 2C), indicative of the more ruptured granules in these systems. Their G'_{final} and $G'_{setback}$ values were consequently lower than the SPI/PS 8:6 sample (Fig. 2C), probably due to the less gel-strengthening impacts of the CS and GS fragments.

3.2. Molecular interactions involved in the plant-based omelets

Common protein-starch interactions in the food systems include H-bonding, electrostatic interactions, and van der Waals forces (Lu et al.,

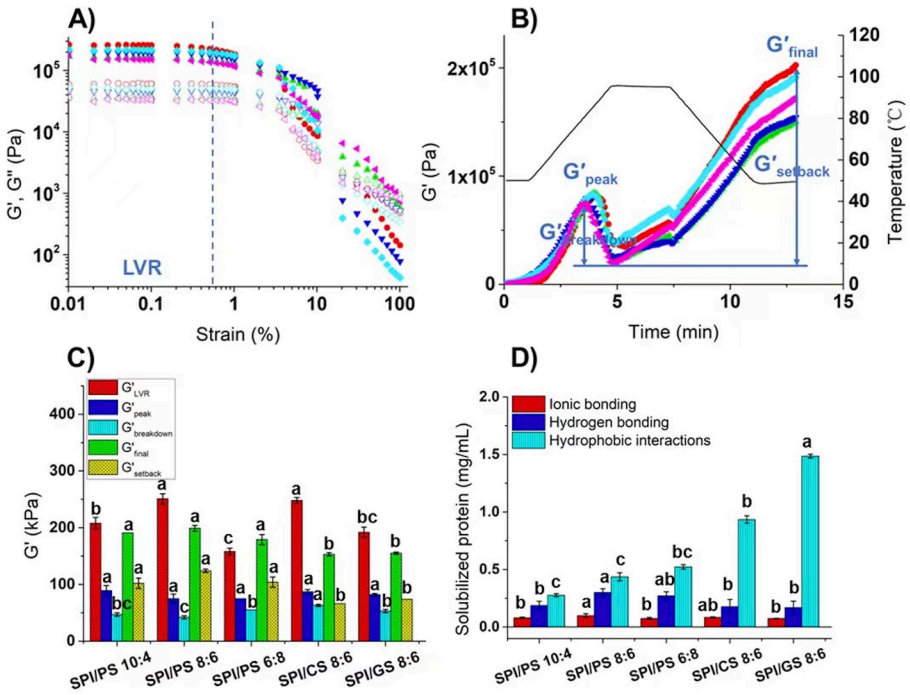

Fig. 2. Storage modulus G' and loss modulus G" from the strain sweep (A); Storage modulus G' from the temperature sweep (B); Summary of G'_{LVR}, G'_{peak}, $G'_{breakdown}$, G'_{fianl}, and $G'_{setback}$ obtained from the strain sweep and the temperature sweep (C); The molecular interactions (expressed as solubilized protein concentration (mg/mL)) of the plant-based omelets (D). *●, SPI/PS 8:6 G'; ▲, SPI/CS 8:6 G'; ▼, SPI/GS 8:6 G'; ◆, SPI/PS 10:4 G'; ◀, SPI/PS 6:8 G'; ○, SPI/PS 8:6 G"; △, SPI/CS 8:6 G"; ▽, SPI/GS 8:6 G"; ◇, SPI/PS 10:4 G"; ◁, SPI/PS 6:8 G". *Groups with different lowercase letters indicate significant difference ($P < 0.05$) among samples; For the same sample, groups with different capital letters indicate significant difference ($P < 0.05$) among different treatments. *SPI/PS 8:6, SPI/CS 8:6, SPI/GS 8:6, SPI/PS 10:4, and SPI/PS 6:8 refer to the plant-based eggs with the addition of 8 % soy protein isolate and 6 % potato starch, 8 % soy protein isolate and 6 % corn starch, 8 % soy protein isolate and 6 % glutinous rice starch, 10 % soy protein isolate and 4 % potato starch, and 6 % soy protein isolate and 8 % potato starch (w/w), respectively.

2016). In the current study, the plant-based omelets were treated with NaCl, urea, and 2-mercaptoethanol to investigate the ionic bonding, hydrophobic interactions, hydrogen bonding, and disulfide bonding. The molecular interactions involved were reflected by the solubilized protein content after dissociations (Fig. 2D).

As shown in Fig. 2D, hydrophobic interactions increased with the increased PS proportion, and those in the CS- and GS-modified omelets were higher than those in the PS-modified omelet. These interactions were mainly involved in the heat-induced protein gelling process, during which proteins denatured, exposed the buried hydrophobic residues, aggregated, and constituted a three-dimensional network. Our results indicated that PS additions at the ratio of SPI/PS 10:4 and 8:6 were more likely to interrupt the protein–protein hydrophobic interactions, probably due to their starch granules embedded in the protein network.

Moreover, the hydrogen bonding interactions were the highest in the SPI/PS 8:6 omelet. Previous studies have demonstrated that abundant hydroxyl groups in starch could interact not only with the polar sites (e.g., arginine, asparagine, aspartic acid, glutamic acid, serine, etc.) on the protein side chains, but also with the amine or carbonyl groups on the protein backbones (López-Barón, Gu, Vasanthan, & Hoover, 2017). Yang et al. (2019) also pointed out that hydrogen bonds were the main molecular interactions between whey protein isolate and corn starch. Our results showed that the hydrogen bonding interactions in the SPI/PS 8:6 system were superior to other PS additive amount (SPI/PS 10:4, SPI/PS 6:8) and other starch types (SPI/CS 8:6, SPI/GS 8:6) (Fig. 2D), verifying the most predominant protein-starch interactions in SPI/PS 8:6 as discussed in the viscoelastic behaviors.

Similarly, the SPI/PS 8:6 omelet involved the greatest ionic bonding. It was reported that the phosphate groups in starch would ionize and make the starch negatively charged during pasting (Lu et al., 2016). Then the negatively charged starch may bind to the positively charged proteins through electrostatic complexing, which could diminish the Coulombic repulsion between amylopectin by neutralizing their negative charges and thus limit the starch swelling (Lu et al., 2016). As mentioned above, PS contained more phosphorus than CS and GS; the resulting more electrostatic interactions in SPI/PS 8:6 (Fig. 2D) let it more pronounced in swelling restriction (lower $G'_{breakdown}$; Fig. 2C). Additionally, the shorter amylopectin chains with more short branch chains in GS (Jane et al., 1999) may also hinder the interactions in SPI/GS 8:6.

Furthermore, the FTIR spectra of the native starch (PS, CS, GS), the no starch-modified sample (0starch), and the starch-modified samples (SPI/PS 8:6, SPI/CS 8:6, SPI/GS 8:6, SPI/PS 10:4, SPI/PS 6:8) (Fig. 3A) were collected to verify the interactions between the starch and the plant-based systems. The native starch spectra exhibited characteristic peaks at 3434 cm^{-1} and 2929 cm^{-1}, representing the O—H and C—H stretching vibrations in glucose (Ji et al., 2015). In addition, the 1155 cm^{-1} peak assigned to P═O stretching, and the 852 cm^{-1} peak assigned to P—O stretching (Dong & Cui, 2021) were more apparent in PS, largely due to its higher phosphorus content. The 0starch spectrum exhibited absorption peaks at 1659 cm^{-1} (C═O stretching (amide I)) and 1536 cm^{-1} (N—H bending (amide II)), both of which were identified as the fingerprints of soy proteins (Dong & Cui, 2021). Moreover, the peak at 1376 cm^{-1} was related to the C—N stretching and N—H bending (amide III). The spectra of the starch-modified samples did not present any new peak compared to the above-mentioned spectra, implying that there was no new covalent interaction between the added starch and the plant-based egg systems. However, the relative intensities of the amide I (1659 cm^{-1}), amide II (1536 cm^{-1}), and the phosphate (1155 cm^{-1}) peaks in the starch-modified samples were significantly lower than those in the 0starch and native starch samples, respectively (Fig. 3B). This confirmed the above finding that electrostatic interactions occurred between the negatively charged phosphate groups of starch and the positively charged amino groups of proteins during the gelation process of the plant-based eggs.

3.3. Structural changes of starches in the plant-based egg systems

The FTIR spectra could also elucidate the structural change in starch at molecular level. As shown in the spectra of the starch-modified samples (Fig. 3A), peak positions did not shift significantly among all groups, which indicated that modification with different types or different amount of starch may not change the skeletal conformations of the plant-based eggs significantly. The paramount difference was noted in the peak intensities (Fig. 3B).

It was found that the relative intensities of the 1021, 1083, and 3434

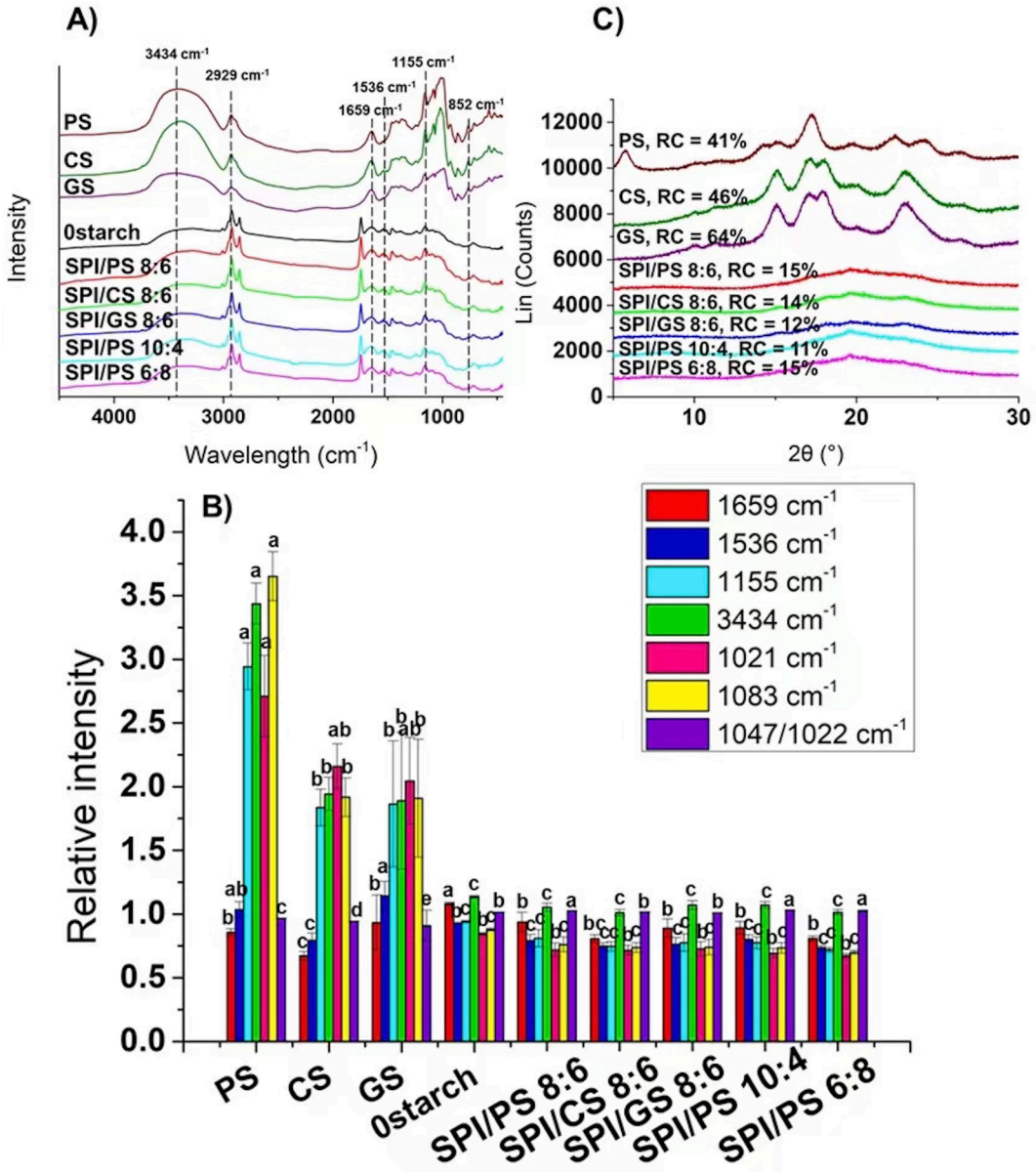

Fig. 3. FTIR spectra of native potato starch (PS), corn starch (CS), glutinous rice starch (GS), no starch-modified sample (0starch), and starch-modified samples (A); Relative intensities of peaks at 1659, 1536, 1155, 3434, 1021, 1083 cm^{-1}, and IR ratio of 1047/1022 cm^{-1} (B); XRD diffractogram of native PS, CS, GS, and different plant-based egg samples (C). *Groups with different letters indicate significant difference ($P < 0.05$). *PS, CS, GS, 0starch, SPI/PS 8:6, SPI/CS 8:6, SPI/GS 8:6, SPI/PS 10:4, and SPI/PS 6:8 refer to native potato starch, native corn starch, native glutinous rice starch, no starch-modified plant-based egg, and the plant-based eggs with the addition of 8 % soy protein isolate and 6 % potato starch, 8 % soy protein isolate and 6 % corn starch, 8 % soy protein isolate and 6 % glutinous rice starch, 10 % soy protein isolate and 4 % potato starch, and 6 % soy protein isolate and 8 % potato starch (w/w), respectively.

cm^{-1} peaks of the plant-based egg samples were lower than those of the pure starch (Fig. 3B). While the peaks at 1021 and 1083 cm^{-1} (anhydroglucose ring C—O stretching) could reflect the hydrogen bonding interactions between the starch chains, the peak at 3434 cm^{-1} (O—H band) could represent the inter- or intra-chain —OH in starch (Ji et al., 2015). The relative intensities results suggested that the inter-chain hydrogen bonding declined when the starch was subjected to the plant-based egg systems. This can happen when —OH groups oriented initially towards the starch chains participated in the H-bonding interactions with the protein molecules (Lin et al., 2017).

To examine the short-range ordering of starch, the infrared (IR) ratio of the 1047/1022 cm^{-1} peaks was calculated (Fig. 3B) after deconvoluting the 1200–800 cm^{-1} region. Compared to those of the native starch, the 1047/1022 cm^{-1} ratios of the plant-based samples enhanced significantly, probably due to the above discussions that in the plant-based egg systems, proteins can adhere to the starch chains, which may act as crosslinkers that improve the molecular orders (Lin et al., 2017). In addition, the IR ratios of the 1047/1022 cm^{-1} peaks in the PS-modified samples were significantly higher than those in the CS- or GS-modified samples, indicating the higher degree of short-range ordering in double helix structures after the modification with PS.

Along with the short-range ordering monitored by FTIR, the XRD spectra (Fig. 3C) elaborated the longer-range ordered structures of starch. Native CS and GS exhibited diffraction peaks at 2θ of 15°, 17°, 18°, and 23°, corresponding to the typical type-A crystalline pattern. Native PS presented the type-B pattern (2θ of 6°, 15°, 17°, 20°, 22°, 24°, and 26°). The relative crystallinity (RC) of GS (63.67 %) was higher than that of CS (46.30 %) and PS (40.55 %). When the native starches were subject to the plant-based egg systems, only one broad diffraction peak at 2θ of 20° was observed (Fig. 3C), matching the V-type amylose–lipid

crystalline diffractogram. The absence of other peaks with respect to the native starch spectra might arise from the swelling and gelatinization of amylose during mixing (Hesso et al., 2015).

In all the plant-based egg systems, the RC values were as low as 10–15 % (Fig. 3C), complying with the relatively low crystallization of starch in the presence of protein and lipid (Wang et al., 2020). It is noteworthy that the RC of SPI/PS 8:6 (15.01 %) was superior to that of SPI/CS 8:6 (13.97 %) and SPI/GS 8:6 (11.81 %), reaching agreement with the short-range ordering results from FTIR. This observation could be associated with the previous presumption that most starch granules were embedded in the protein networks of SPI/PS 8:6, which limited their rapid swelling that caused the destabilization, disorganization, and disruption of the crystalline lamellae (Karapantsios, Sakonidou, & Raphaelides, 2002). Despite the distinctness in determining scope between FTIR (sensitive to short-range ordering) and XRD (longer-range crystallinity) as reported earlier (Lin et al., 2017), consensus on these methods was reached in the present study.

3.4. Microstructures

The microstructures of SPI/PS 10:4, SPI/PS 8:6, SPI/PS 6:8, SPI/CS 8:6, and SPI/GS 8:6 were observed via SEM (Fig. 4). It was shown that the PS-modified samples (SPI/PS 10:4, SPI/PS 8:6, SPI/PS 6:8) made elongated and the largest clusters (indicated by yellow arrows in Fig. 4B), the CS-modified sample (SPI/CS 8:6) appeared as smaller clusters (indicated by yellow arrows in Fig. 4D), and the GS-modified sample (SPI/GS 8:6) exhibited more round clusters (indicated by yellow arrows in Fig. 4E). The larger clusters in the PS-modified omelets were conducive to their cohesive mouthfeel (Fig. 1B) as the components tend to cling together and agglomerate to propagate the elastic deformations (Whitaker et al., 2019; Wang et al., 2017). As for the SPI/PS ratios, SPI/PS 10:4 displayed more large and irregular pores (indicated by white arrows in Fig. 4A); this resulted in its loose structure and soft mouthfeel (Fig. 1A). With the increasing PS proportion, the sizes of the pores were reduced, and the distributions were more regular; this allowed the more compact and intensive structures of the SPI/PS 8:6 and 6:8 gels. It is maybe that PS compacted and tightened the structures by interacting with SPI and filling in the SPI networks; a phenomenon similar to the rice starch filled inside the protein matrix of the imitation cheese (Mounsey & O'Riordan, 2008). However, SPI/PS 6:8 possessed an over-compact structure, where many starch granules may escape from the SPI networks (indicated by white arrows in Fig. 4C) and led to

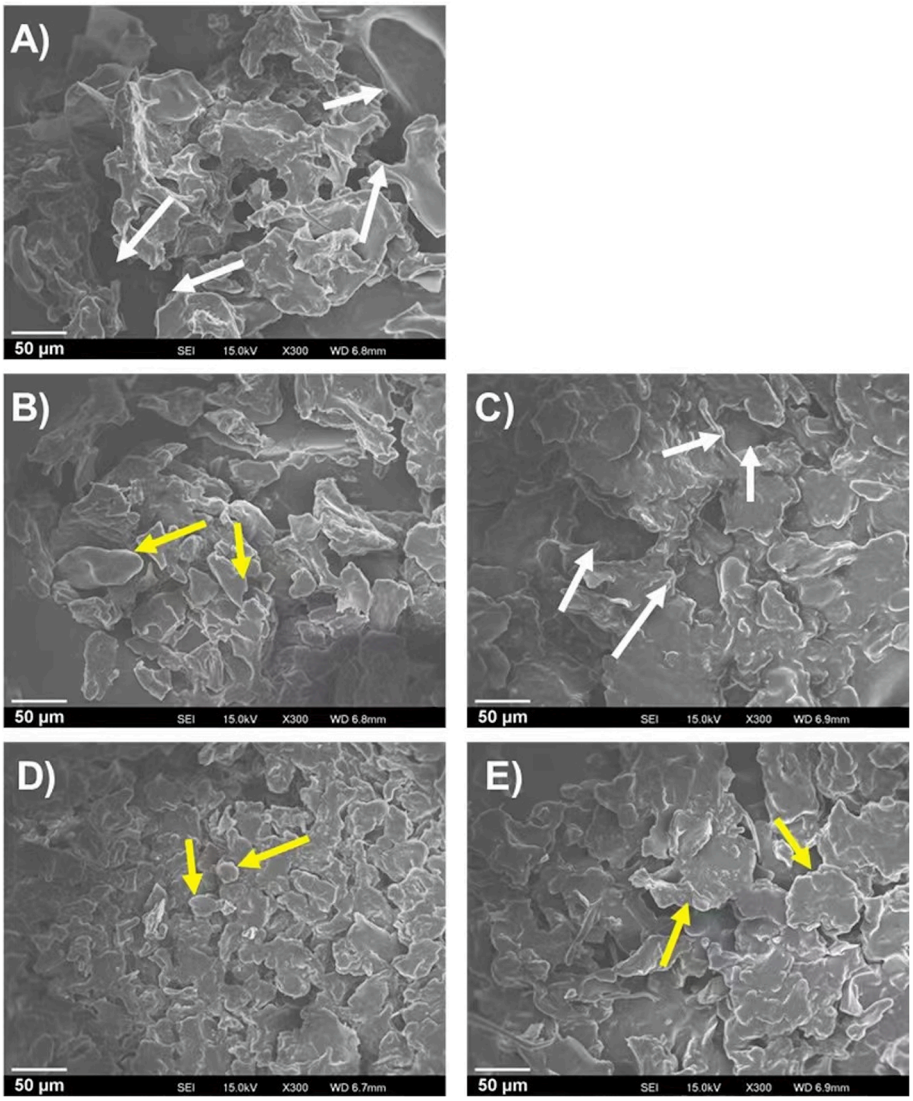

Fig. 4. SEM images of A) SPI/PS 10:4, B) SPI/PS 8:6, C) SPI/PS 6:8, D) SPI/CS 8:6, and E) SPI/GS 8:6. *SPI/PS 8:6, SPI/CS 8:6, SPI/GS 8:6, SPI/PS 10:4, and SPI/PS 6:8 refer to the plant-based eggs with the addition of 8% soy protein isolate and 6% potato starch, 8% soy protein isolate and 6% corn starch, 8% soy protein isolate and 6% glutinous rice starch, 10% soy protein isolate and 4% potato starch, and 6% soy protein isolate and 8% potato starch (w/w), respectively.

the higher $G'_{breakdown}$ during heating (Fig. 2C).

3.5. Schematic diagram

A schematic diagram based on all the results above was proposed to elucidate the roles of starch in the plant-based egg systems (Fig. 5). Different natures of starch can trigger different interactions and structures in the plant-based egg samples, thereby contributing to their different physicochemical properties. PS, in virtue of its greater phosphorus content than CS and GS, could induce more protein-starch electrostatic interactions. In addition, the more hydroxyl groups of PS that were engaged in hydrogen bonding formation between starch chains or protein-starch resulted in the higher hydrogen bonding interactions observed in SPI/PS 8:6 than those in SPI/CS 8:6 and SPI/GS 8:6. As a result of the highest hydrogen bonding and electrostatic interactions in SPI/PS 8:6, a structure with the most starch granules embedded in the protein networks was expected (Fig. 5), which could limit starch swelling and rupture during heating, and thus lead to the least $G'_{breakdown}$, the higher short-range ordering, and the greatest relative crystallinity in SPI/PS 8:6. These more intact and ordered starch granules, as fillers, were able to further strengthen the gel structures and give rise to the highest gel strength of SPI/PS 8:6. It turned out that the superiority in interactions and structures allowed SPI/PS 8:6 to successfully match the texture of native egg omelet.

Regarding the adding amount of PS, a critical ratio of SPI/PS at 8:6 was notable. When a system contained less PS and more SPI (SPI/PS 10:4), there were insufficient inlaid starch granules for reinforcing the gel networks; as a result, SPI/PS 10:4 delivered a lower gel strength and cannot achieve the desirable texture as the native egg omelet. When a system contained more PS and less SPI (SPI/PS 6:8), the proteins were not enough to enwrap the excessive starch, which were not as effective in protecting starch from swelling and rupture as those in SPI/PS 8:6. This was responsible for the higher $G'_{breakdown}$, the less crystallized starch structures, the lower gel strength, and the lower cohesiveness of SPI/PS 6:8.

3.5.1. Model validation by in vitro digestion analysis

The characteristic ^{1}H spectrum of the plant-based egg (SPI/PS 8:6) after *in vitro* digestion is displayed in Fig. S1. Most of the signal peaks were within 0.5–5.5 ppm, where typical metabolites (e.g., amino acids, aliphatic acids, saccharides, etc.) were found (Huang et al., 2021). Twenty-eight metabolites, including fatty acids, amino acids, and saccharides, were identified through the 1D and 2D spectra (Fig. S1, Table S1). To be specific, the ^{1}H signal peaks in 0.8–3.0 ppm were allocated to amino acids (e.g., isoleucine, leucine) and fatty acids (e.g., linoleic acid, palmitic acid), those in 3.0–5.5 ppm were mainly allocated to soluble saccharides (e.g., α-D-glucose, β-D-glucose, sucrose, maltose, and fructose), and those in 6.5–8.0 ppm were allocated to amino acids (e.g., tyrosine, tryptophan, and phenylalanine). Such identified metabolites were generally in line with the plant-based egg compositions that were rich in proteins, carbohydrates, and lipids, as well as the *in vitro* digestive metabolites reported in other foods (e.g., sponge cake (Huang et al., 2021), fish (Vidal et al., 2016), and cheese (Bordoni et al., 2011)).

To explore the similarities and dissimilarities in the metabolite profile of the plant-based egg samples, the supervised PCA was performed (Fig. S2). The quality parameters ($R^2X = 0.94$, $Q^2 = 0.64 > 0.50$; Fig. S2A) reflected the reliable interpretation and prediction of the model. As demonstrated in the PCA score plot (Fig. S2B), samples from the same group were well clustered, while samples from the different group were clearly deviated from each other. This pointed out the diverse metabolite release patterns of the different plant-based eggs. Furthermore, the PCA loading plot (Fig. S2C) represented the metabolite loading contributing to such group separation. Majority of the metabolites (e.g., methionine, linoleic acid, serine, etc.) were largely loaded on PC2, while several metabolites (e.g., alanine and linoleic acid) exhibited notable loading on PC1 and PC3, respectively. These metabolites were

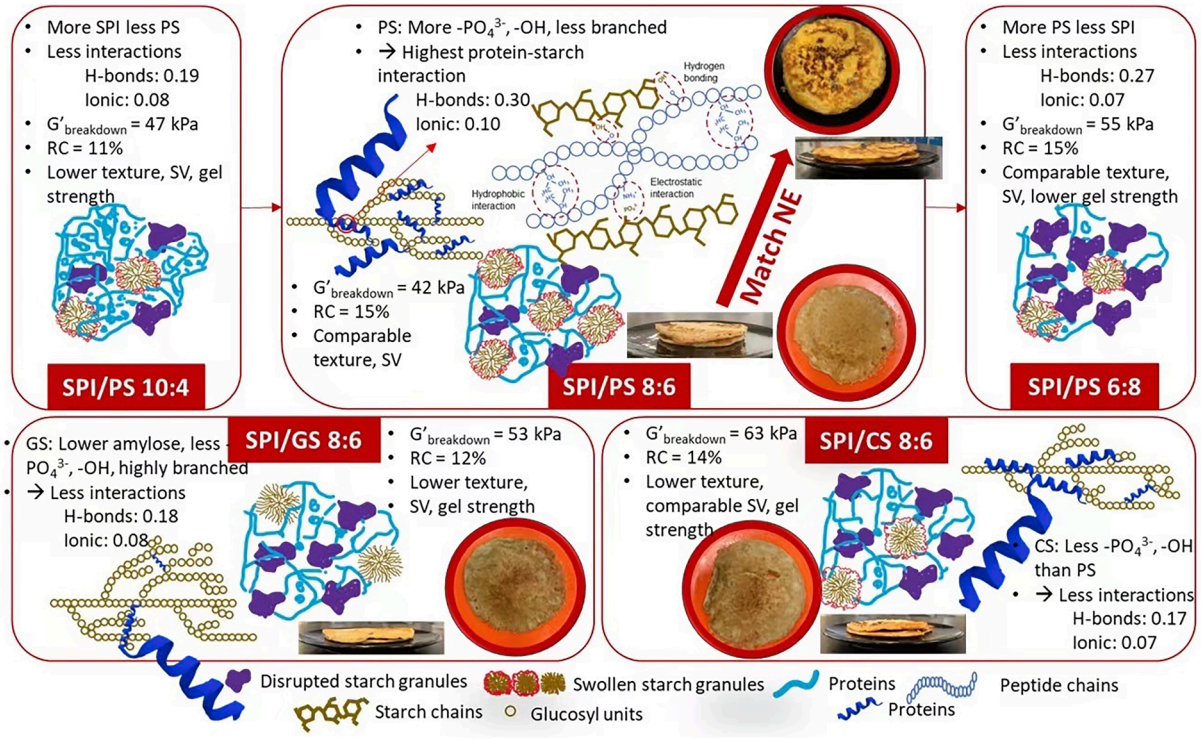

Fig. 5. Schematic diagram connecting the physicochemical properties, molecular interactions, and microstructures of the plant-based eggs modified by different starch. *SPI/PS 8:6, SPI/CS 8:6, SPI/GS 8:6, SPI/PS 10:4, and SPI/PS 6:8 refer to the plant-based eggs with the addition of 8% soy protein isolate and 6% potato starch, 8% soy protein isolate and 6% corn starch, 8% soy protein isolate and 6% glutinous rice starch, 10% soy protein isolate and 4% potato starch, and 6% soy protein isolate and 8% potato starch (w/w), respectively. *SV, specific volume; RC, relative crystallinity.

regarded as "marker metabolites" responding to the addition of different starch into the plant-based egg systems (Huang et al., 2021).

To further elucidate the discrepancy in metabolite release between SPI/PS 8:6 and other plant-based egg samples, the supervised OPLS-DA was performed on the SPI/PS 8:6 and SPI/PS 10:4 group, the SPI/PS 8:6 and SPI/PS 6:8 group, the SPI/PS 8:6 and SPI/CS 8:6 group, and the SPI/PS 8:6 and SPI/GS 8:6 group (Fig. 6). All the established models displayed reliable interpretation and prediction (R^2X = 0.76–0.88, Q^2 = 0.97–0.99). It was shown from the OPLS-DA score plots (Fig. 6A'-D') that clear separations occurred between SPI/PS 8:6 and other plant-based egg groups, confirming the significant changes in metabolite release due to the modification with different starch. For the sake of investigating the significant metabolites that accounted for the separations of the pairwise groups, volcano plots recording the FCs, the *P* values, and the VIP values of the metabolites were developed (Fig. 6A''-D''). A metabolite with FC > 1.5 and $P < 0.05$ was regarded as statistically significant (Ran, Yang, Chen, & Yang, 2022). According to these criteria, there were 6, 3, 3, and 5 significant increasing metabolites ($\log_{1.5}$ FC > 1, $-\log P > 1.3$) released from SPI/PS 10:4, SPI/PS 6:8, SPI/CS 8:6, and SPI/GS 8:6, respectively, as compared to SPI/PS 8:6. These significant increasing metabolites mainly comprised several amino acids (Pro, Val, Ser) and fatty acid (LA), which could be ascribed to the increasing digestibility of proteins and lipids. As discussed above, the greatest molecular interactions and RC in SPI/PS 8:6 contributed to its relatively rigid structure with the highest gel strength; this enabled it to resist from enzymatic digestion (Fig. 6E''') and to release less metabolites. On the other hand, the loose gel structures with the lower gel strength owing to the less molecular interactions, lower RC, and higher $G'_{breakdown}$ in SPI/PS 10:4, SPI/PS 6:8, SPI/CS 8:6, and SPI/GS 8:6 (Fig. 6A'''-D''') could accelerate the enzyme diffusivity (Luo, Ye, Wolber, & Singh, 2021), protein dissolution and oil release (Guo, Ye, Lad, Dalgleish, & Singh, 2014); this facilitated the digestibility of these samples and led to their higher metabolite release. Previous works targeting on the relationship of gel structures and *in vitro* digestibility also found a lower digestibility of proteins, lipids (Guo et al., 2014; Luo et al., 2021) and starch (Yin et al., 2021) in the firmer gels, possibly due to their retarding disintegration, trivial oil coalescence, impeditive protein hydrolysis, and/or resistant complex formations. Apart from that, the type-B crystallinity, the smaller surface/volume granular structure, and the highly resistant retrograded amylose in PS were conducive to the resistant starch formations (Sajilata, Singhal, & Kulkarni, 2006), which could further interact with the proteins or lipids to hinder the digestions (Opazo-Navarrete, Tagle Freire, Boom, & Janssen, 2019; Ran et al., 2022). The superior resistant starch content in PS could also explain the reduced release of several amino acids (Ser, Pro, Ala, Val) and fatty acid (LA) from SPI/PS 8:6 in comparison of those from SPI/CS 8:6 or SPI/GS 8:6 (Fig. 6C'', D''). Overall, the results of NMR-based metabolite release from *in vitro* digestion verified the schematic diagram proposed in

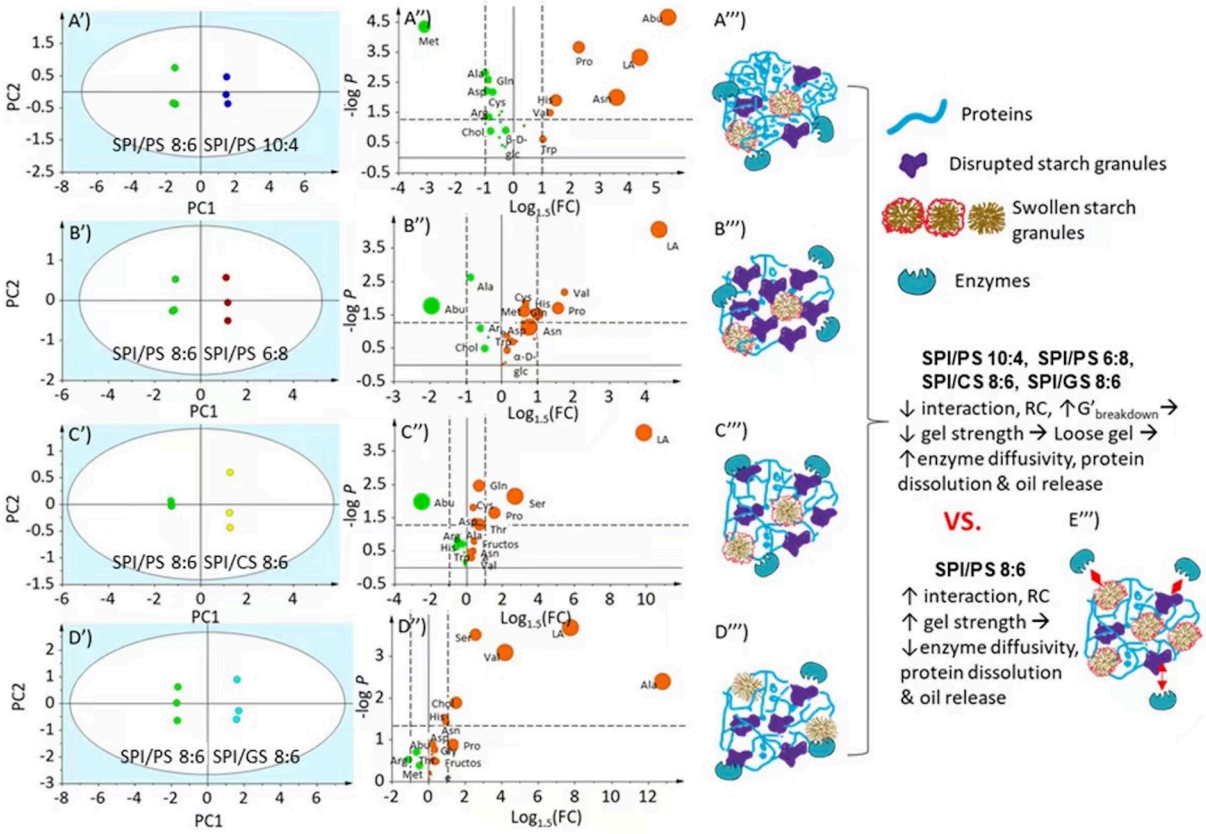

Fig. 6. OPLS-DA score plots of SPI/PS 8:6 and SPI/PS 10:4 (A'), SPI/PS 8:6 and SPI/PS 6:8 (B'), SPI/PS 8:6 and SPI/CS 8:6 (C'), SPI/PS 8:6 and SPI/GS 8:6 (D'); Volcano plots of SPI/PS 8:6 and SPI/PS 10:4 (A''), SPI/PS 8:6 and SPI/PS 6:8 (B''), SPI/PS 8:6 and SPI/CS 8:6 (C''), SPI/PS 8:6 and SPI/GS 8:6 (D''); Schematic diagrams of SPI/PS 10:4 (A'''), SPI/PS 6:8 (B'''), SPI/CS 8:6 (C'''), SPI/GS 8:6 (D'''), and SPI/PS 8:6 (E''') during *in vitro* digestion. *Green color in the volcano plots represented decreasing metabolites compared to SPI/PS 8:6, while orange color in the volcano plots represented increasing metabolites compared to SPI/PS 8:6. *Size of the circles indicated the VIP values. *LA, linoleic acid; OA, oleic acid; PA, palmitic acid; Ile, isoleucine; Leu, leucine; Val, valine; Ala, alanine; Arg, arginine; Thr, threonine; Pro, proline; Gln, glutamine; Met, methionine; Cys, cysteine; Asp, aspartic acid; Abu, aminobutyric acid; Asn, asparagine; Chol, choline; Gly, glycine; Ser, serine; β-D-glc, β-D-glucose; α-D-glc, α-D-glucose; Tyr, tyrosine; Phe, phenylalanine; Trp, tryptophan; His, histidine. *SPI/PS 8:6, SPI/CS 8:6, SPI/GS 8:6, SPI/PS 10:4, and SPI/PS 6:8 refer to the plant-based eggs with the addition of 8% soy protein isolate and 6% potato starch, 8% soy protein isolate and 6% corn starch, 8% soy protein isolate and 6% glutinous rice starch, 10% soy protein isolate and 4% potato starch, and 6% soy protein isolate and 8% potato starch (w/w), respectively. (For interpretation of the references to color in this figure legend, the reader is referred to the web version of this article.)

section 3.4.

4. Conclusion

In conclusion, this study enunciated the impacts of starch on the physicochemical properties of the plant-based eggs by exploring the molecular interactions in protein-starch and the structural changes in starch. Modification with SPI/PS at 8:6 improved the hardness, springiness, cohesiveness, chewiness, and specific volume of the plant-based omelet to a commensurate level as the native egg omelet. SPI/PS 8:6 involved the greatest electrostatic and hydrogen bonding interactions, owing mainly to the higher content of phosphorus and hydroxyl groups in PS. Such interactions contributed to a relatively strong structure with most intact starch granules filled inside the protein networks, and these protein barriers could protect PS from swelling and rupture, giving the most intact (the lowest $G'_{breakdown}$) and crystallized (the highest RC) starch structures in SPI/PS 8:6. In virtue of the preponderant interactions and structures, SPI/PS 8:6 omelet can successfully mimic the physicochemical properties of the native egg omelet. CS and GS, however, were less efficient in supporting the gel structures as PS, thereby failing to match the texture of the native egg omelet. Furthermore, the PS addition ratio at SPI/PS 8:6 appeared to be more effective than that at SPI/PS 10:4 or SPI/PS 6:8. This was due to inadequate amounts of starch granules embedded in the protein networks in SPI/PS 10:4, and excess starch granules in SPI/PS 6:8 such that the proteins were insufficient to encase all of them. The metabolite release from *in vitro* digestion validated the proposed schematic models, by demonstrating that less metabolites (especially several amino acids and fatty acid) were released from the sample with the highest gel strength (SPI/PS 8:6). With the deepened understanding on the starch behaviors in the plant-based egg systems, this study provided more insight in modifying the food properties using different starch. Future studies regarding the effects of other types of starch (e.g., tapioca starch, wheat starch, etc.) could be investigated to further improve the mouthfeel of plant-based omelets.

CRediT authorship contribution statement

Zhou Lu: Conceptualization, Methodology, Investigation, Software, Visualization, Validation, Writing – original draft, Writing – review & editing. **Yi Liu:** Conceptualization, Methodology. **Yi En Jayne Lee:** Methodology, Investigation, Software. **Andrew Chan:** Methodology, Investigation, Visualization, Writing – review & editing. **Pin-Rou Lee:** Methodology. **Hongshun Yang:** Conceptualization, Funding acquisition, Project administration, Supervision, Writing – review & editing.

Declaration of Competing Interest

The authors declare that they have no known competing financial interests or personal relationships that could have appeared to influence the work reported in this paper.

Data availability

Data will be made available on request.

Acknowledgements

This study was funded by National Research Foundation Singapore SYNERGY Seed Grant (A-8000508-00-00).

Appendix A. Supplementary data

Supplementary data to this article can be found online at https://doi.org/10.1016/j.foodchem.2022.134390.

References

Alexander, S. (1998). Amorphous solids: Their structure, lattice dynamics and elasticity. *Physics Reports, 296*(2–4), 65–236.
Bordoni, A., Picone, G., Babini, E., Vignali, M., Danesi, F., Valli, V., … Capozzi, F. (2011). NMR comparison of *in vitro* digestion of Parmigiano Reggiano cheese aged 15 and 30 months. *Magnetic Resonance in Chemistry, 49*(S1), S61–S70.
Bühler, J. M., Schlangen, M., Möller, A. C., Bruins, M. E., & van der Goot, A. J. (2022). Starch in plant-based meat replacers: A new approach to using endogenous starch from cereals and legumes. *Starch-Stärke, 74*(1–2), 2100157.
Dong, D., & Cui, B. (2021). Fabrication, characterization and emulsifying properties of potato starch/soy protein complexes in acidic conditions. *Food Hydrocolloids, 115*, 106600.
Grasso, N., Alonso-Miravalles, L., & O'Mahony, J. A. (2020). Composition, physicochemical and sensorial properties of commercial plant-based yogurts. *Foods, 9*(3), 252.
Guo, Q., Ye, A., Lad, M., Dalgleish, D., & Singh, H. (2014). Effect of gel structure on the gastric digestion of whey protein emulsion gels. *Soft Matter, 10*(8), 1214–1223.
Hesso, N., Le-Bail, A., Loisel, C., Chevallier, S., Pontoire, B., Queveau, D., & Le-Bail, P. (2015). Monitoring the crystallization of starch and lipid components of the cake crumb during staling. *Carbohydrate Polymers, 133*, 533–538.
Huang, M., Zhao, X., Mao, Y., Chen, L., & Yang, H. (2021). Metabolite release and rheological properties of sponge cake after *in vitro* digestion and the influence of a flour replacer rich in dietary fibre. *Food Research International, 144*, 110355.
Jane, J., Chen, Y., Lee, L., McPherson, A., Wong, K., Radosavljevic, M., & Kasemsuwan, T. (1999). Effects of amylopectin branch chain length and amylose content on the gelatinization and pasting properties of starch. *Cereal Chemistry, 76*(5), 629–637.
Jekle, M., Mühlberger, K., & Becker, T. (2016). Starch–gluten interactions during gelatinization and its functionality in dough like model systems. *Food Hydrocolloids, 54*, 196–201.
Ji, N., Li, X., Qiu, C., Li, G., Sun, Q., & Xiong, L. (2015). Effects of heat moisture treatment on the physicochemical properties of starch nanoparticles. *Carbohydrate Polymers, 117*, 605–609.
Kamani, M. H., Meera, M. S., Bhaskar, N., & Modi, V. K. (2019). Partial and total replacement of meat by plant-based proteins in chicken sausage: Evaluation of mechanical, physico-chemical and sensory characteristics. *Journal of Food Science and Technology, 56*(5), 2660–2669.
Karapantsios, T. D., Sakonidou, E. P., & Raphaelides, S. N. (2002). Water dispersion kinetics during starch gelatinization. *Carbohydrate Polymers, 49*(4), 479–490.
Li, S., Wei, Y., Fang, Y., Zhang, W., & Zhang, B. (2014). DSC study on the thermal properties of soybean protein isolates/corn starch mixture. *Journal of Thermal Analysis and Calorimetry, 115*(2), 1633–1638.
Lin, M., Tay, S. H., Yang, H., Yang, B., & Li, H. (2017). Development of eggless cakes suitable for lacto-vegetarians using isolated pea proteins. *Food Hydrocolloids, 69*, 440–449.
López-Barón, N., Gu, Y., Vasanthan, T., & Hoover, R. (2017). Plant proteins mitigate *in vitro* wheat starch digestibility. *Food Hydrocolloids, 69*, 19–27.
Lu, Z., Lee, P. R., & Yang, H. (2022). Chickpea flour and soy protein isolate interacted with κ-carrageenan via electrostatic interactions to form egg omelets analogue. *Food Hydrocolloids*, 107691.
Lu, Z.-H., Donner, E., Yada, R. Y., & Liu, Q. (2016). Physicochemical properties and *in vitro* starch digestibility of potato starch/protein blends. *Carbohydrate Polymers, 154*, 214–222.
Luo, N., Ye, A., Wolber, F. M., & Singh, H. (2021). Effect of gel structure on the *in vitro* gastrointestinal digestion behaviour of whey protein emulsion gels and the bioaccessibility of capsaicinoids. *Molecules, 26*(5), 1379.
Mattice, K. D., & Marangoni, A. G. (2020). Physical properties of plant-based cheese products produced with zein. *Food Hydrocolloids, 105*, 105746.
McGee, H. (2007). *On food and cooking: The science and lore of the kitchen*. New York: Simon and Schuster.
Mishra, S., & Rai, T. (2006). Morphology and functional properties of corn, potato and tapioca starches. *Food Hydrocolloids, 20*(5), 557–566.
Moreno, H. M., Domínguez-Timón, F., Díaz, M. T., Pedrosa, M. M., Borderías, A. J., & Tovar, C. A. (2020). Evaluation of gels made with different commercial pea protein isolate: Rheological, structural and functional properties. *Food Hydrocolloids, 99*, 105375.
Mounsey, J. S., & O'Riordan, E. (2008). Characteristics of imitation cheese containing native or modified rice starches. *Food Hydrocolloids, 22*(6), 1160–1169.
Opazo-Navarrete, M., Tagle Freire, D., Boom, R. M., & Janssen, A. E. M. (2019). The influence of starch and fibre on *in vitro* protein digestibility of dry fractionated quinoa seed (Riobamba variety). *Food Biophysics, 14*(1), 49–59.
Ran, X., Yang, Z., Chen, Y., & Yang, H. (2022). Konjac glucomannan decreases metabolite release of a plant-based fishball analogue during *in vitro* digestion by affecting amino acid and carbohydrate metabolic pathways. *Food Hydrocolloids, 129*, 107623.
Sajilata, M. G., Singhal, R. S., & Kulkarni, P. R. (2006). Resistant starch–a review. *Comprehensive Reviews in Food Science and Food Safety, 5*(1), 1–17.
Schirmer, M., Höchstötter, A., Jekle, M., Arendt, E., & Becker, T. (2013). Physicochemical and morphological characterization of different starches with variable amylose/amylopectin ratio. *Food Hydrocolloids, 32*(1), 52–63.
Shao, Y., Lin, K., & Chen, Y. (2015). Batter and product quality of eggless cakes made of different types of flours and gums. *Journal of Food Processing and Preservation, 39*(6), 2959–2968.
Su, Y., Dong, Y., Niu, F., Wang, C., Liu, Y., & Yang, Y. (2015). Study on the gel properties and secondary structure of soybean protein isolate/egg white composite gels. *European Food Research and Technology, 240*(2), 367–378.

Sui, Z., Yao, T., Zhao, Y., Ye, X., Kong, X., & Ai, L. (2015). Effects of heat–moisture treatment reaction conditions on the physicochemical and structural properties of maize starch: Moisture and length of heating. *Food Chemistry, 173*, 1125–1132.

Vidal, N. P., Picone, G., Goicoechea, E., Laghi, L., Manzanos, M. J., Danesi, F., … Guillén, M. D. (2016). Metabolite release and protein hydrolysis during the *in vitro* digestion of cooked sea bass fillets. A study by ^{1}H NMR. *Food Research International, 88*, 293–301.

Wang, S., Chao, C., Cai, J., Niu, B., Copeland, L., & Wang, S. (2020). Starch–lipid and starch–lipid–protein complexes: A comprehensive review. *Comprehensive Reviews in Food Science and Food Safety, 19*(3), 1056–1079.

Wang, W., Chen, W., Yang, H., & Cui, M. (2017). Textural and rheological properties of potato starch as affected by amino acids. *International Journal of Food Properties, 20* (sup3), S3123-S3134.

Whitaker, K. A., Varga, Z., Hsiao, L. C., Solomon, M. J., Swan, J. W., & Furst, E. M. (2019). Colloidal gel elasticity arises from the packing of locally glassy clusters. *Nature Communications, 10*(1), 1–8.

Yang, C., Zhong, F., Douglas Goff, H., & Li, Y. (2019). Study on starch-protein interactions and their effects on physicochemical and digestible properties of the blends. *Food Chemistry, 280*, 51–58.

Yin, X., Zheng, Y., Kong, X., Cao, S., Chen, S., Liu, D., … Tian, J. (2021). RG-I pectin affects the physicochemical properties and digestibility of potato starch. *Food Hydrocolloids, 117*, 106687.

Youssef, M. K., & Barbut, S. (2011). Effects of two types of soy protein isolates, native and preheated whey protein isolates on emulsified meat batters prepared at different protein levels. *Meat Science, 87*(1), 54–60.

Zhang, M., Li, J., Su, Y., Chang, C., Li, X., Yang, Y., & Gu, L. (2019). Preparation and characterization of hen egg proteins-soybean protein isolate composite gels. *Food Hydrocolloids, 97*, 105191.

Zhang, T., Li, Z., Wang, Y., Xue, Y., & Xue, C. (2016). Effects of konjac glucomannan on heat-induced changes of physicochemical and structural properties of surimi gels. *Food Research International, 83*, 152–161.